

M₃Ag₁₇(SPh)₁₂ Nanoparticles and Their Structure Prediction

Sameera Wickramasinghe,[†] Aydar Atnagulov,[†] Bokwon Yoon,[§] Robert N. Barnett,[§] Wendell P. Griffith,[†] Uzi Landman,[§] and Terry P. Bigioni^{*,†,‡}

[†]Department of Chemistry and [‡]The School of Solar and Advanced Renewable Energy, University of Toledo, Toledo, Ohio 43606, United States

[§]School of Physics, Georgia Institute of Technology, Atlanta, Georgia 30332-0430, United States

S Supporting Information

ABSTRACT: Although silver nanoparticles are of great fundamental and practical interest, only one structure has been determined thus far: M₄Ag₄₄(SPh)₃₀, where M is a monocation, and SPh is an aromatic thiolate ligand. This is in part due to the fact that no other molecular silver nanoparticles have been synthesized with aromatic thiolate ligands. Here we report the synthesis of M₃Ag₁₇(4-*tert*-butylbenzene-thiol)₁₂, which has good stability and an unusual optical spectrum. We also present a rational strategy for predicting the structure of this molecule. First-principles calculations support the structural model, predict a HOMO–LUMO energy gap of 1.77 eV, and predict a new “monomer mount” capping motif, Ag(SR)₃, for Ag nanoparticles. The calculated optical absorption spectrum is in good correspondence with the measured spectrum. Heteroatom substitution was also used as a structural probe. First-principles calculations based on the structural model predicted a strong preference for a single Au atom substitution in agreement with experiment.

Silver nanoparticles are of significant fundamental and practical interest because of their optical and biological properties. Nevertheless, very little is known about the principles that govern their structures. The precise atomic structures of molecular nanoparticles can be determined by single-crystal X-ray diffraction methods; however, only one silver nanoparticle structure has been determined by single-crystal X-ray diffraction methods thus far: M₄Ag₄₄(SPh)₃₀, where M is a single-charge cationic counterion, and SPh is a thiolate ligand containing a phenyl ring.^{1–4} This provided the first picture of the silver thiolate protective outer layer, which was shown to consist of 3D Ag₂(SPh)₅ mounts.¹ These mounts are very different from the 1D staple motif in the case of thiolate-ligated gold nanoparticles.^{5–8} It remains to be seen, however, whether the Ag₂(SPh)₅ mounts are common to a variety of thiolated silver nanoparticles or whether they are unique for protecting the 32 Ag atom excavated decahedral core of M₄Ag₄₄(SPh)₃₀. Such information is critically important for understanding the principles behind silver nanoparticle structures and developing a general structural model for thiolated silver nanoparticles as well as self-assembled monolayers on silver surfaces.

A large number of phenyl-ring-containing ligands have been used to prepare M₄Ag₄₄(SPh)₃₀ nanoparticles.³ Interestingly,

preparations of M₄Ag₄₄(SPh)₃₀ nanoparticles have yet to yield other species; all appear to be single-sized products. It is somewhat of a challenge, then, to produce other species that may be crystallized for comparison in structural studies because phenyl-ring-containing ligands are important for crystallization. To this end, we have used a bulky phenyl-ring-containing ligand, 4-*tert*-butylbenzenethiol (TBBT), to change the interligand interactions and thereby induce the formation of a new silver nanoparticle species. Herein we report the synthesis of M₃Ag₁₇(TBBT)₁₂ nanoparticles, their salient physical properties, and a compelling structural model that introduces a new silver thiolate mount motif.

The M₃Ag₁₇(TBBT)₁₂ nanoparticles were synthesized by a method that was similar to a previous report.³ Silver nitrate (0.714 mmol) was dissolved along with TBBT (0.500 mmol) in 7.20 mL of dimethylformamide (DMF) and then stirred for 15 min. This mixture formed a yellow precipitate, which was the silver thiolate precursor. The precursor was reduced with 28.6 mL of a DMF solution of NaBH₄ (2.86 mmol), which was added dropwise. The cloudy yellow mixture changed to form a clear orange solution that darkened over time as it was stirred for 3 h. The color at this stage was dominated by larger plasmonic species, as verified by absorption spectroscopy;⁴ however, a new peak was also present near 443 nm (Figure S3). Next, 4.20 mL of deionized water was added to increase the reduction potential of the NaBH₄. This also sped up the reaction; therefore, the solution was left to incubate for 16 h at –18 °C. Over this time, a dark precipitate formed, and the optical density of the solution decreased. Presumably, the precipitate was formed from the larger silver nanoparticles that were observed before the addition of water. The final solution was clear and yellow in color.

The product of this reaction was analyzed by electrospray-ionization mass spectrometry (ESI-MS), which revealed the presence of a new silver nanoparticle: Ag₁₇(TBBT)₁₂^{3–} (Figure 1). Such a species has not been observed in any other preparation of silver molecular nanoparticles with either aromatic^{1–3,9} or aliphatic^{10–12} thiolate ligands. Only a small amount of one fragment species was observed, namely, Ag₁₇(TBBT)₁₁^{2–}, indicating that Ag₁₇(TBBT)₁₂^{3–} was quite stable for the conditions of the measurement (Figure S1). No charge state distribution was observed because the TBBT ligand is aprotic. Other species observed included adducts of

Received: May 31, 2015

Published: August 24, 2015



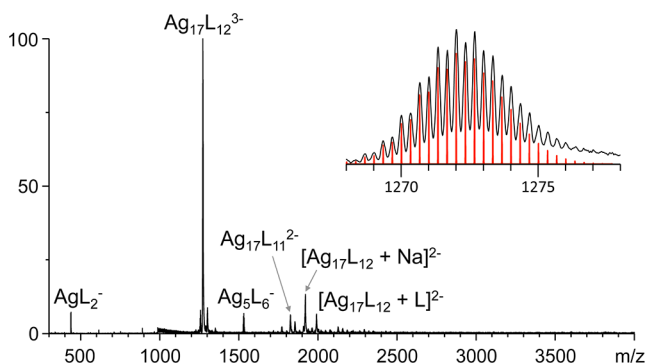


Figure 1. Electrospray-ionization mass spectrum of Ag:TBBT nanoparticles, showing $\text{Ag}_{17}(\text{TBBT})_{12}^{3-}$ along with other species. Inset: experimental (black) and simulated (red) isotopic patterns for $\text{Ag}_{17}\text{L}_{12}^{3-}$, where L = TBBT, with a shift of 0.08 m/z to correct for a 63 ppm mass difference due to external calibration.

the parent compound along with $\text{Ag}(\text{TBBT})_2^-$ and $\text{Ag}_5(\text{TBBT})_6^-$, which may have been solution-phase decomposition products.¹³ No $\text{Ag}_{44}(\text{TBBT})_{30}^{4-}$ was observed, consistent with optical measurements.

The dark-yellow supernatant had a single strong absorption peak located at 424 nm that dominated the optical absorption spectrum, unlike any previously observed, with two small features on either side and a slowly decaying low-energy tail (Figures 3 and S4). The prominent peak at 424 nm is much narrower (0.18 eV fwhm) and located to the red of a typical plasmon peak characteristic of a spherical silver nanoparticle.^{14,15} None of the spectral features characteristic of $\text{Na}_4\text{Ag}_{44}(\text{TBBT})_{30}$ were observed in the spectrum, which is consistent with the ESI-MS results.

X-ray data are not always available for structure determination; therefore, structure prediction methods are needed. The prediction of structures of gold and silver molecular nanoparticles presents one of the foremost challenges in molecular nanoparticle science, however, and has yet to yield a definite successful example. The small size of $\text{M}_3\text{Ag}_{17}(\text{TBBT})_{12}$ as well as past lessons learned provide an opportunity to begin the formulation of guiding principles for structure prediction and to attempt the prediction of a verifiable structure of this molecular nanoparticle.

First, it is well-known that very small metal particles tend to assume low-energy icosahedral structures.^{16,17} Gold and silver molecular nanoparticles share this tendency because the cores of many known structures contain icosahedra, with few exceptions; therefore, it is reasonable to begin a structural model with an icosahedral core. Second, it is also well-known that the presence of a central atom in the icosahedral core affects primarily the superatomic S orbitals because of their nonzero amplitude at the origin, i.e., the center of the particle.^{18–20} For example, an 18-electron spherical core will have 1S^2 , 1P^6 , and 1D^{10} occupied orbitals and a 2S orbital as the lowest unoccupied molecular orbital (LUMO);²¹ therefore, an empty 12-atom icosahedron would be favored because it would raise the energy of the 2S LUMO and thereby increase the energy gap. This is the case for $\text{M}_4\text{Ag}_{44}(\text{SPh})_{30}$.^{1,2}

Formal counting²² for $\text{M}_3\text{Ag}_{17}(\text{TBBT})_{12}$ nanoparticles gives eight delocalized electrons, which are expected to fill the 1S^2 and 1P^6 orbitals²¹ so that the highest occupied molecular orbital (HOMO) is 1P and the LUMO is 1D. This is indeed found from our density functional theory (DFT) electronic

structure calculations (see below); therefore, there is no electronic advantage to an empty 12-atom icosahedral core. This is generally the case for an eight-electron core, such as $\text{MAu}_{25}(\text{SR})_{18}$.^{6,7} In contrast, there is an energetic advantage to a 13-atom (atom-centered) icosahedral core because of the coordination of the central atom. We therefore predict $\text{Na}_3\text{Ag}_{17}(\text{TBBT})_{12}$ to have a 13-atom icosahedral core, as shown in Figure 2a.

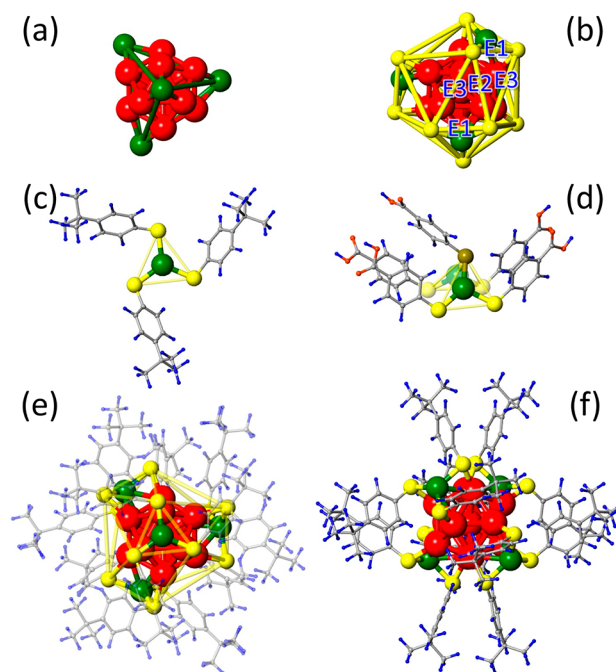


Figure 2. Proposed structure for $\text{M}_3\text{Ag}_{17}(\text{TBBT})_{12}$ nanoparticles, constructed and relaxed with DFT calculations. (a) The structure consists of an icosahedral Ag_{13} core (red) capped with four tetrahedrally located Ag atoms (green). (b) Twelve sulfur atoms (yellow) surround the silver core, with three S atoms forming an equilateral triangle around each tetrahedrally located Ag atom, to form a distorted icosahedron (yellow lines); E1, E2, and E3 are different edge lengths. (c) Isolated view of a $\text{Ag}(\text{TBBT})_3$ monomer unit structure; the S atoms form an equilateral triangle (yellow lines). Carbon atoms are gray, and hydrogen atoms are blue. (d) Isolated view of the $\text{Ag}_2(\text{pMBA})_5$ dimer mount structure found on the $\text{Na}_4\text{Ag}_{44}(\text{pMBA})_{30}$ molecule; for comparison see ref 1. The S atoms form nearly equilateral triangles (yellow lines); oxygen atoms are in orange. (e) View of the $\text{M}_3\text{Ag}_{17}(\text{TBBT})_{12}$ structure down the threefold axis, showing slight rotation between the mount and the underlying icosahedral core. (f) View showing face-to-face interactions of the phenyl rings of ligands on neighboring mounts, leading to an overall octahedral arrangement of ligand bundles.

Next, we consider the ligand shell. In the case of gold molecular nanoparticles, the capping motif has consistently been shown to be monomer and dimer staples.^{5–8} These can be thought of as fragments of the linear gold thiolate polymer, $p\text{-(AuSR)}_n$. For silver, the capping motif for $\text{M}_4\text{Ag}_{44}(\text{SPh})_{30}$ nanoparticles was carefully analyzed and has been shown to be the aforementioned $\text{Ag}_2(\text{SPh})_5$ mount.¹ This is a 3D structure and is therefore distinct from the linear gold thiolate polymer. The fact that $\text{Ag}_2(\text{SPh})_5$ mounts were observed instead of staples can be understood on the basis of the topological difference between the bonding of gold and silver in metal thiolates, which are two- and three-coordinate, respectively.²³

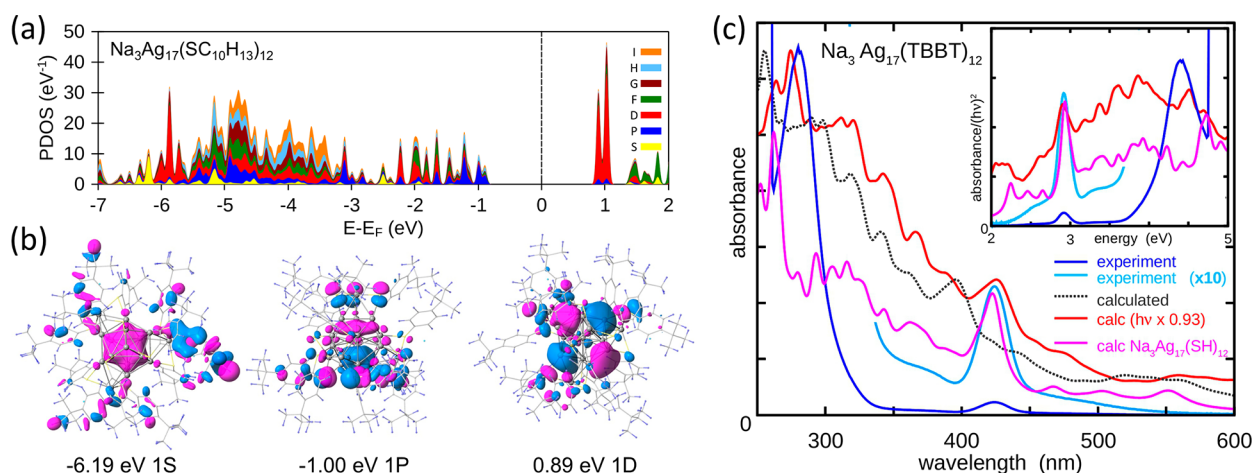


Figure 3. Electronic properties. (a) Projected DOS calculated for the relaxed $\text{Na}_3\text{Ag}_{17}(\text{TBBT})_{12}$ structure. The color-coded angular momenta are given on the right. (b) Representative wave function portraits corresponding to the indicated energies are given at the bottom. (Blue and purple signify different signs.) The nodal structures for the delocalized orbitals with eigenenergies -6.19 , -1.00 , and 0.89 eV correspond to 1S, 1P (HOMO) and 1D (LUMO) superatom states. The Fermi energy, at $E_F = 0.0$ eV, is indicated by the dashed line. (c) Measured (dark and light-blue lines) and TD-DFT-calculated (red and dotted black lines) optical absorption spectra of $\text{Na}_3\text{Ag}_{17}(\text{TBBT})_{12}$ nanoparticles and calculated spectrum for $\text{Na}_3\text{Ag}_{17}(\text{SH})_{12}$ (pink) plotted vs wavelength and energy (inset). The dotted black line is the as-calculated spectrum, and the red line is obtained by scaling the as-calculated spectrum.

Using this example, the 4 Ag atoms and 12 ligands that remain after accounting for the Ag_{13} core can be grouped into 4 trigonal quasi-planar $\text{Ag}(\text{SPh})_3$ mounts, as shown in Figure 2c. These can be thought of as fragments of the 2D silver-thiolate polymer.²⁴ In fact, the $\text{Ag}(\text{SPh})_3$ mount could be considered to be the primitive capping unit for silver thiolate ligands because $\text{Ag}_2(\text{SPh})_5$ mounts can be constructed by fusing two $\text{Ag}(\text{SPh})_3$ mounts. (See Figure 2d, where two of the newly proposed $\text{Ag}(\text{SPh})_3$ mounts are joined at the apex S atom with the elimination of a single thiolate.) In analogy to monomer and dimer staples for gold thiolate ligands,^{5–8} the $\text{Ag}(\text{SPh})_3$ and $\text{Ag}_2(\text{SPh})_5$ capping units can be thought of as monomer and dimer mounts.

Because icosahedra contain the tetrahedral symmetry group, it is possible to arrange the four trigonal planar $\text{Ag}(\text{SPh})_3$ mounts symmetrically around the Ag_{13} core, as shown in Figure 2e. Structural optimization of the molecule with the use of first-principles relaxation revealed that interactions between ligands on neighboring mounts lead to ligand pair bundling,²⁵ resulting in a ligand shell structure with an overall octahedral arrangement (Figure 2f). Here, the ligands tilt in order to maximize the interligand interaction, thereby facilitating face-to-face interactions between the rings with minimal interference from the *tert*-butyl groups. This ligand pair bundling and the symmetry that it confers on the ligand shell are likely to assist in the crystallization of these molecular nanoparticles and influence the properties of the resulting superlattice.²⁶

The stability of the proposed structure is strongly supported by the results of our DFT calculations (Supporting Information), which reveal a density of states (DOS) with a large HOMO–LUMO energy gap $E_{\text{gap}} = 1.77$ eV (Figure 3a). Such a large predicted gap is consistent with experimental ESI-MS measurements of marked gas-phase stability (Supporting Information). Furthermore, the projection of the wave functions onto their angular momenta components shows the expected superatom shell structure with occupied 1S^2 and HOMO 1P^6 delocalized orbitals and superatom LUMO 1D orbitals. (See wave function portraits in Figure 3b.)

The calculated time-dependent DFT (TD-DFT) optical absorption spectrum (Supporting Information, section S5) is in good correspondence with the measured one, lending further support to the proposed structural model (Figure 3c). The experimental spectrum was measured in DMF, and the theoretical spectrum was calculated in vacuum. Thus, redshift-scaling was applied to the calculated spectrum to simulate a solvatochromic effect so that the main prominent absorption feature near 400 nm matched (Figures 3c and S6). The observed absorption features for $\text{M}_3\text{Ag}_{17}(\text{TBBT})_{12}$ are at (A) 424 nm (2.92 eV) and (B) at 280 nm (4.43 eV). For $\text{M}_3\text{AuAg}_{16}(\text{TBBT})_{12}$ these features are found at (A') 408 nm (3.04 eV) and (B') 281 nm (4.41 eV) (Figure S6).

In the calculated spectrum for $\text{Na}_3\text{Ag}_{17}(\text{TBBT})_{12}$, the main absorption features are at (A) 396 nm (3.13 eV) and (B) at 256 nm (4.85 eV). Feature A at 396 nm (3.13 eV) originates from (i) occupied states at -2.33 eV lying mostly on the phenyl rings, excited to the LUMO (0.89 eV) and LUMO+1 1D superatom states on the metal core, (ii) occupied states on the sulfur and silver (d states) atoms at -1.97 eV, excited to the 1D superatom states, and (iii) the HOMO superatom 1P state excited to unoccupied states at 2.30 eV on the phenyl ring. For feature B, the calculated peak occurs at 256 nm (4.85 eV), and it originates from (i) phenyl π -states at -2.31 eV, excited to π^* states at 2.51 eV hybridized in part with sulfur states, (ii) d-band Ag and sulfur states at -1.97 eV, excited to phenyl and ligand states at 2.81 eV, and (iii) d-band metal states at -3.7 to -3.9 eV, excited to the unoccupied 1D superatom states near 1.01 eV.

The calculated spectrum for $\text{Na}_3\text{Ag}_{17}(\text{SH})_{12}$ (pink in Figure 3c) illustrates enhancement of the main observed spectral features (peaks A and B) by suppressing contributions from transitions involving ligand states. (See the region between 300 to 400 nm.) The latter are expected to be more susceptible to smearing of spectral features because of solvent effects and fluctuations, as evidenced in the solution-phase spectra.

Heteroatom substitution was used as a structural probe of $\text{M}_3\text{Ag}_{17}(\text{TBBT})_{12}$. DFT calculations using our model structure predicted a strong preference for a single Au atom substitution

(0.89 eV stabilization for an optimal geometry with the central Ag atom substituted), accompanied by a gap of $E_{\text{gap}} = 1.81$ eV, compared to 1.83 eV for a two-atom Au substitution and 1.77 eV for the all-Ag structure which was confirmed by experiment. Namely, when a stoichiometric 1:16 Au/Ag input ratio was used, $\text{M}_3\text{AuAg}_{16}(\text{TBBT})_{12}$ was produced with only a minor component of $\text{M}_3\text{Au}_2\text{Ag}_{15}(\text{TBBT})_{12}$; no $\text{M}_3\text{Ag}_{17}(\text{TBBT})_{12}$ was detected. When a fivefold excess of Au was used (5:16 Au/Ag input ratio), the results of the synthesis were unchanged. (See Supporting Information for details.)

We have presented experimental results showing the existence of $\text{M}_3\text{Ag}_{17}(\text{TBBT})_{12}$. The structure of this new molecular silver nanoparticle is predicted to consist of a Ag_{13} icosahedral core that is surrounded by a tetrahedral arrangement of newly found $\text{Ag}(\text{SPh})_3$ planar mounts. A rational strategy for predicting the structure of this molecule and calculations that support the structural model were discussed. This work presents an important step toward the goal of developing accurate predictive structural models in order to relieve the crystallization bottleneck that currently limits the structural data available for silver and other metals.

■ ASSOCIATED CONTENT

● Supporting Information

The Supporting Information is available free of charge on the ACS Publications website at DOI: 10.1021/jacs.5b05422.

Additional details regarding the syntheses, ESI-MS measurements, and theoretical analyses are supplied as Supporting Information. (PDF)

■ AUTHOR INFORMATION

Corresponding Author

*E-mail: Terry.Bigioni@utoledo.edu.

Notes

The authors declare no competing financial interest.

■ ACKNOWLEDGMENTS

We thank Dr. Constantine Yannouleas for helpful discussions. Work at the University of Toledo was supported by NSF grant CBET-0955148 and the School of Solar and Advanced Renewable Energy. B.Y. was supported by grant FA9550-14-1-0005 from the Air Force Office of Scientific Research, and R.N.B. and U.L. by the Office of Basic Energy Sciences of the US Department of Energy under contract no. FG05-86ER45234. Calculations were carried out at the Georgia Tech Center for Computational Materials Science.

■ REFERENCES

- (1) Desireddy, A.; Conn, B. E.; Guo, J.; Yoon, B.; Barnett, R. N.; Monahan, B. M.; Kirschbaum, K.; Griffith, W. P.; Whetten, R. L.; Landman, U.; Bigioni, T. P. *Nature* **2013**, *501*, 399–402.
- (2) Yang, H.; Wang, Y.; Huang, H.; Gell, L.; Lehtovaara, L.; Malola, S.; Häkkinen, H.; Zheng, N. *Nat. Commun.* **2013**, *4*, 2422.
- (3) Bakr, O. M.; Amendola, V.; Aikens, C. M.; Wenseleers, W.; Li, R.; Dal Negro, L.; Schatz, G. C.; Stellacci, F. *Angew. Chem., Int. Ed.* **2009**, *48*, 5921–5926.
- (4) Conn, B. E.; Desireddy, A.; Atmagulov, A.; Wickramasinghe, S.; Bhattarai, B.; Yoon, B.; Barnett, R. N.; Abdollahian, Y.; Kim, Y. W.; Griffith, W. P.; Oliver, S. R. J.; Landman, U.; Bigioni, T. P. *J. Phys. Chem. C* **2015**, *119*, 11238–11249.
- (5) Jadzinsky, P. D.; Calero, G.; Ackerson, C. J.; Bushnell, D. A.; Kornberg, R. D. *Science* **2007**, *318*, 430–433.

- (6) Heaven, M. W.; Dass, A.; White, P. S.; Holt, K. M.; Murray, R. W. *J. Am. Chem. Soc.* **2008**, *130*, 3754–3755.
- (7) Zhu, M.; Aikens, C. M.; Hollander, F. J.; Schatz, G. C.; Jin, R. *J. Am. Chem. Soc.* **2008**, *130*, 5883–5885.
- (8) Qian, H.; Eckenhoff, W. T.; Zhu, Y.; Pintauer, T.; Jin, R. *J. Am. Chem. Soc.* **2010**, *132*, 8280–8281.
- (9) Chakraborty, I.; Kurashige, W.; Kanehira, K.; Gell, L.; Häkkinen, H.; Negishi, Y.; Pradeep, T. *J. Phys. Chem. Lett.* **2013**, *4*, 3351–3355.
- (10) Cathcart, N.; Kitaev, V. *J. Phys. Chem. C* **2010**, *114*, 16010–16017.
- (11) Kumar, S.; Bolan, M. D.; Bigioni, T. P. *J. Am. Chem. Soc.* **2010**, *132*, 13141–13143.
- (12) Chakraborty, I.; Govindarajan, A.; Erusappan, J.; Ghosh, A.; Pradeep, T.; Yoon, B.; Whetten, R. L.; Landman, U. *Nano Lett.* **2012**, *12*, 5861–5866.
- (13) Desireddy, A.; Kumar, S.; Guo, J.; Bolan, M. D.; Griffith, W. P.; Bigioni, T. P. *Nanoscale* **2013**, *5*, 2036–2044.
- (14) Mulvaney, P. *Langmuir* **1996**, *12*, 788–800.
- (15) Peng, S.; McMahon, J. M.; Schatz, G. C.; Gray, S. K.; Sun, Y. *Proc. Natl. Acad. Sci. U. S. A.* **2010**, *107*, 14530–14534.
- (16) Frank, F. C. *Proc. R. Soc. London, Ser. A* **1952**, *215*, 43–46.
- (17) Kelton, K. F.; Lee, G. W.; Gangopadhyay, A. K.; Hyers, R. W.; Rathz, T. J.; Rogers, J. R.; Robinson, M. B.; Robinson, D. S. *Phys. Rev. Lett.* **2003**, *90*, 195504.
- (18) Zhang, S. B.; Cohen, M. L.; Chou, M. Y. *Phys. Rev. B: Condens. Matter Mater. Phys.* **1987**, *36*, 3455–3458.
- (19) Baladron, C.; Alonso, J. A. *Phys. B* **1988**, *154*, 73–81.
- (20) Yannouleas, C.; Jena, P.; Khanna, S. N. *Phys. Rev. B: Condens. Matter Mater. Phys.* **1992**, *46*, 9751–9760.
- (21) Knight, W. D.; Clemenger, K.; de Heer, W. A.; Saunders, W. A.; Chou, M. Y.; Cohen, M. L. *Phys. Rev. Lett.* **1984**, *52*, 2141–2143.
- (22) Walter, M.; Akola, J.; Lopez-Acevedo, O.; Jadzinsky, P. D.; Calero, G.; Ackerson, C. J.; Whetten, R. L.; Gronbeck, H.; Häkkinen, H. *Proc. Natl. Acad. Sci. U. S. A.* **2008**, *105*, 9157–9162.
- (23) Dance, I. G. *Polyhedron* **1986**, *5*, 1037–1104.
- (24) Dance, I. G.; Fisher, K. J.; Banda, R. M. H.; Scudder, M. L. *Inorg. Chem.* **1991**, *30*, 183–187.
- (25) Luedtke, W. D.; Landman, U. *J. Phys. Chem.* **1996**, *100*, 13323–13329.
- (26) Yoon, B.; Luedtke, W. D.; Barnett, R. N.; Gao, J.; Desireddy, A.; Conn, B. E.; Bigioni, T. P.; Landman, U. *Nat. Mater.* **2014**, *13*, 807–811.
- (27) AbdulHalim, L. G.; Bootharaju, M. S.; Tang, Q.; Del Gobbo, S.; AbdulHalim, R. G.; Eddaoudi, M.; Jiang, D.-e.; Bakr, O. M. *J. Am. Chem. Soc.* **2015**, DOI: 10.1021/jacs.5b04547.

■ NOTE ADDED IN PROOF

The structure of a 29-atom silver nanoparticle, which shares many features with our work, was recently brought to our attention.²⁷

SUPPORTING INFORMATION

$M_3Ag_{17}(SPh)_{12}$ Nanoparticles and Their Structure Prediction

Sameera Wickramasinghe,¹ Aydar Atmagulov,¹ Bokwon Yoon,² Robert N. Barnett,² Wendell P. Griffith,¹ Uzi Landman,² and Terry P. Bigioni^{1,3*}

¹Department of Chemistry, University of Toledo, Toledo, Ohio 43606, ²School of Physics, Georgia Institute of Technology, Atlanta, GA 30332-0430, and ³The School of Solar and Advanced Renewable Energy, University of Toledo, Toledo, Ohio 43606.

*E-mail: Terry.Bigioni@utoledo.edu

Experimental Methodology

S1 - Chemicals: Sodium borohydride and N,N-dimethylformamide (DMF) were purchased from Fisher Chemical. Silver nitrate, gold (III) chloride trihydrate, and 4-*tert*-butylbenzenethiol (TBBT) were purchased from Sigma-Aldrich. All the reagents were used without further purification. Deionized water (18.2 M Ω cm) from a Millipore Synergy system was used.

S2 - Synthesis of $M_3Ag_{17}(SR)_{12}$ and $M_3AuAg_{16}(SR)_{12}$: The synthesis of $M_3Ag_{17}(SR)_{12}$ was based upon a synthesis that was reported elsewhere.¹ First, 121 mg of silver nitrate (0.714 mmol) was dissolved in 7.20 mL DMF and stirred for 5 min. Next, 86 μ L of TBBT (0.500 mmol) were added to the solution, which was stirred for an additional 15 min. The silver-thiolate precursor formed during this time. A 28.60 mL DMF solution containing 108 mg of NaBH₄ (2.85 mmol) was added drop wise to the reaction mixture in order to reduce the precursor. This reaction was allowed to stir at 1100 rpm for 3 h. After this time, 4.20 mL of deionized water was added to the reaction in order to increase the reduction potential of the NaBH₄ and consequently the kinetics. This mixture was stirred for another 2 min before storing in a freezer at -18 °C for 16 h. After 16 h in the freezer, the product was separated into a clear yellow supernatant and a dark precipitate.

The synthesis of $M_3AuAg_{16}(SR)_{12}$ was done in two different ways: (i) with a stoichiometric Au:Ag ratio of 1:16, and (ii) with a “nonstoichiometric” Au:Ag ratio of 5:16, i.e. a five-fold excess of gold. For the stoichiometric (1:16) reaction, 114 mg of silver nitrate (0.672 mmol) and 16.5 mg of gold(III) chloride trihydrate (0.042 mmol) were dissolved in 7.20 mL DMF and stirred for 5 min. Next, 86 μ L of TBBT (0.500 mmol) were added to the solution, which was stirred for an additional 15 min. The metal-thiolate precursor formed during this time. A 28.60

mL DMF solution containing 108 mg of NaBH₄ (2.85 mmol) was added drop wise to the reaction mixture in order to reduce the precursor. This reaction was allowed to stir at 1100 rpm for 3 h. After this time, 4.20 mL of deionized water was added to the reaction in order to increase the reduction potential of the NaBH₄ and consequently the kinetics. This mixture was stirred for another 2 min before storing in a freezer at -18 °C for 16 h. After 16 h in the freezer, the product was separated into a clear orange supernatant and a dark precipitate.

For the 5:16 “nonstoichiometric” reaction, 93 mg of silver nitrate (0.546 mmol) and 66 mg of gold(III) chloride trihydrate (0.168 mmol) were dissolved in 7.20 mL DMF and stirred for 5 min. Next, 86 μL of TBBT (0.500 mmol) were added to the solution, which was stirred for an additional 15 min. The metal-thiolate precursor formed during this time. A 28.60 mL DMF solution of NaBH₄ (0.1080 g, 2.85 mmol) was added drop wise to the reaction mixture in order to reduce the precursor. This reaction was allowed to stir at 1100 rpm for 3 h. After this time, 4.20 mL of deionized water was added to the reaction in order to increase the reduction potential of the NaBH₄ and consequently the kinetics. This mixture was stirred for another 2 min before storing in a freezer at -18 °C for 16 h. After 16 h in the freezer, the product was separated into a violet supernatant and a dark precipitate.

S3 - Electrospray ionization mass spectrometry: All mass spectra were collected on a Waters Synapt HDMS G1 quadrupole time-of-flight mass spectrometer in negative ion V-mode using a nanospray source with fused silica emitters made in house. Instrument parameters used for data collection were as follows: capillary voltage, 2.0-4.0 kV; sampling cone, 15 V; extraction cone, 4.0 V; nanoflow, 0.1 bar; cone gas, 0 L/h; trap collision energy, 0.5 V; transfer collision energy, 1.0 V; source temperature, 40 °C; desolvation temperature, 120 °C. Calibration was performed externally in the range of $100 \leq m/z \leq 4000$ using cesium iodide. MassLynx 4.1 software (Waters Corp.) was used for processing spectra. Simulating isotopic patterns was performed using mMass freeware (copyright Martin Strohmalm).² Samples were taken directly from the reaction mixture and diluted using neat DMF.

The formula of M₃Ag₁₇(TBBT)₁₂ is based upon the requirement that the molecule needs to be neutral in the solid state, wherein 3 monocationic counterions are needed to balance charge of the Ag₁₇(TBBT)₁₂³⁻ ion identified by ESI-MS. It is likely that the counterions are Na⁺ given their abundance in the synthesis, therefore the formula is expected to be Na₃Ag₁₇(TBBT)₁₂.

Gas Phase Stability: Fragmentation of isolated parent ions at low collision energy (see Fig. S1) showed that the Ag₁₇L₁₂³⁻ ion is relatively stable in the gas phase. In order to reduce the charge on metallic core, however, it may undergo a Coulomb explosion. The two observed gas phase reactions can be summarized as:

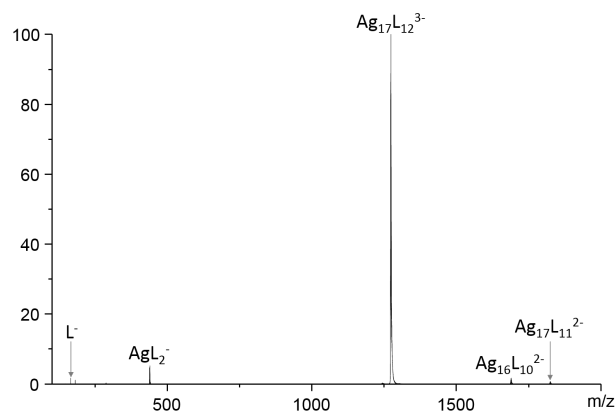
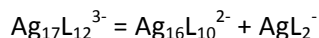
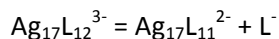


Figure S1. Spontaneous fragmentation (CE = 0.5 eV) of isolated Ag₁₇L₁₂³⁻ ions.



We note that the gas phase stability of the $\text{Ag}_{17}\text{L}_{12}^{3-}$ ion was better than that of the $\text{Ag}_{44}\text{L}_{30}^{4-}$ ion, namely the AgL_2^- and [parent – AgL_2^-] fragment intensities were significantly lower relative to the parent peak in the case of the $\text{Ag}_{17}\text{L}_{12}^{3-}$ ion (compare Fig. S4 and Fig. S2b in Ref. 17). These measurements of the superior gas phase stability of $\text{Ag}_{17}\text{L}_{12}^{3-}$ versus $\text{Ag}_{44}\text{L}_{30}^{4-}$ support our proposed structure model, which predicts better stability due to a larger HOMO-LUMO energy gap of 1.94 eV for $\text{M}_3\text{Ag}_{17}\text{L}_{12}$ versus only 0.78 eV for $\text{M}_4\text{Ag}_{44}\text{L}_{30}$.

Heteroatom substitution was used as a structural probe, to test the validity of our proposed structure. Calculations based on this structure predicted that a single Au atom substitution would be strongly preferred, with a stabilization of 0.89 eV for $\text{M}_3\text{AuAg}_{16}(\text{SR})_{12}$ compared to $\text{M}_3\text{Ag}_{17}(\text{SR})_{12}$ (see below). This is 50% stronger than the 12 Au atom substitution into $\text{M}_4\text{Ag}_{44}(\text{SR})_{30}$ to form $\text{M}_4\text{Ag}_{12}\text{Ag}_{32}(\text{SR})_{30}$, which stabilized the molecule by only 0.61 eV/substituted Au atom, which itself supports the quality of our predicted model. ESI-MS showed that stoichiometric heteroatom substitution (1:16 Au:Ag) into $\text{M}_3\text{Ag}_{17}(\text{SR})_{12}$ produced $\text{M}_3\text{AuAg}_{16}(\text{SR})_{12}$ almost exclusively, with only a small amount of $\text{M}_3\text{Au}_2\text{Ag}_{15}(\text{SR})_{12}$ also found; no $\text{M}_3\text{Ag}_{17}(\text{SR})_{12}$ was observed (see Fig. S2A). This selectivity persisted even when the gold content was increased five-fold; the mass distribution as measured by ESI-MS was unchanged (see Fig. S2B). This is quite different compared to the analogous substitution of Au into $\text{M}_4\text{Ag}_{44}(\text{SR})_{30}$ and Ag into $\text{MAu}_{25}(\text{SR})_{18}$,^{16,18} both of which produce normal distributions of species with different substitutions. The experimental measurement of the exceptional selectivity of the single Au atom substitution is consistent with our prediction that the structure has a central atom within the icosahedron and the DFT prediction of very strong stabilization with a single Au atom substitution, providing further support for our model.

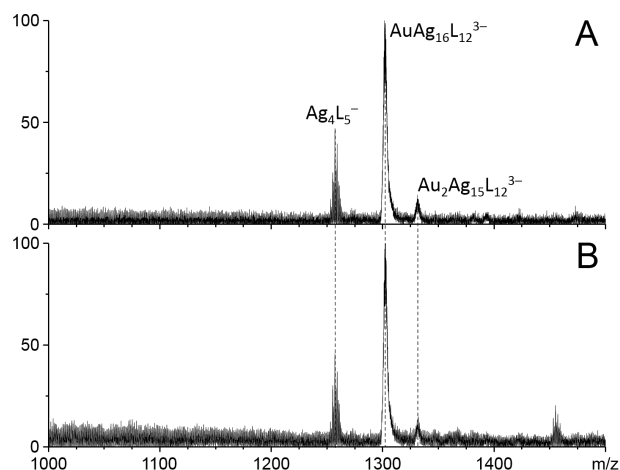


Figure S2. ESI-MS of the product obtained from syntheses using Au:Ag input ratios of (A) 1:16 and (B) 5:16.

S4 - Optical absorption spectroscopy:

All optical absorption spectra were obtained using a PerkinElmer Lambda 950 spectrophotometer with a standard 1.00 mm path length quartz cuvette. An optical absorption spectrum was collected for the reaction mixture before water was added (see Fig. S3) and for the supernatant that was the final product (see Fig. S4 and Fig. 3c of the main text). Although the reaction mixture contained $M_3Ag_{17}(SR)_{12}$ before water was added, the reaction

accelerated and produced only $M_3Ag_{17}(SR)_{12}$ after water addition; no $M_4Ag_{44}(SR)_{30}$ was observed.

Stoichiometric heteroatom substitution (1:16 Au:Ag) into $M_3Ag_{17}(SR)_{12}$ was found to produce $M_3AuAg_{16}(SR)_{12}$ almost exclusively, with only a small amount of $M_3Au_2Ag_{15}(SR)_{12}$ also found. The optical absorption spectrum for this material was similar in nature to that of $M_3Ag_{17}(SR)_{12}$, however the main absorption peak was shifted to higher energy (see Fig. S5).

The “nonstoichiometric” reaction (5:16 Au:Ag) also produced $M_3AuAg_{16}(SR)_{12}$ almost exclusively, with a similarly small amount of $M_3Au_2Ag_{15}(SR)_{12}$ also found. The excess gold instead formed larger plasmonic gold nanoparticles, as can be seen in Fig. S5.

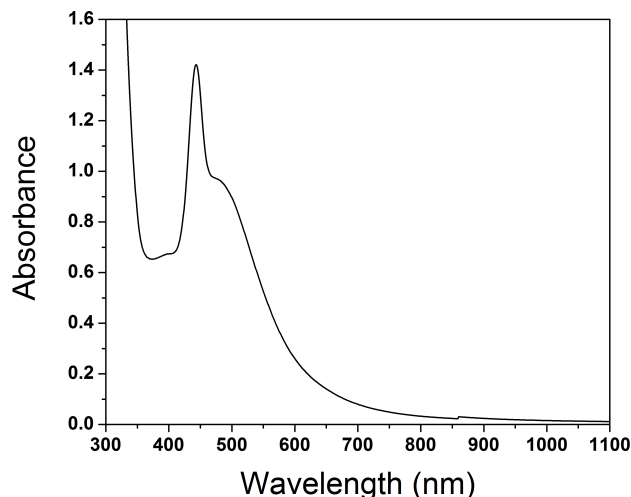


Figure S3. Optical absorption spectrum of the reaction mixture before adding water.

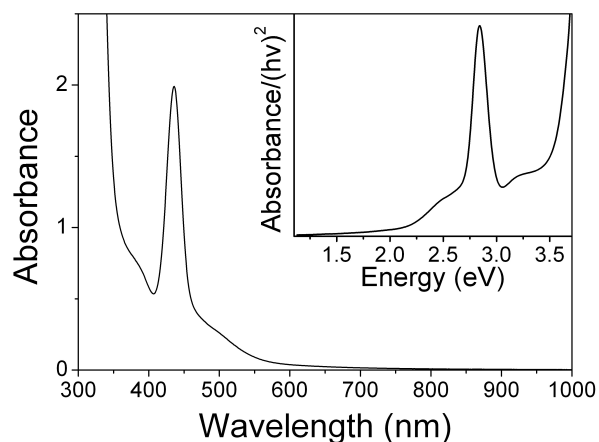


Figure S4. Optical absorption spectrum of $M_3Ag_{17}(TBBT)_{12}$ nanoparticles in DMF. Inset: spectrum in energy.

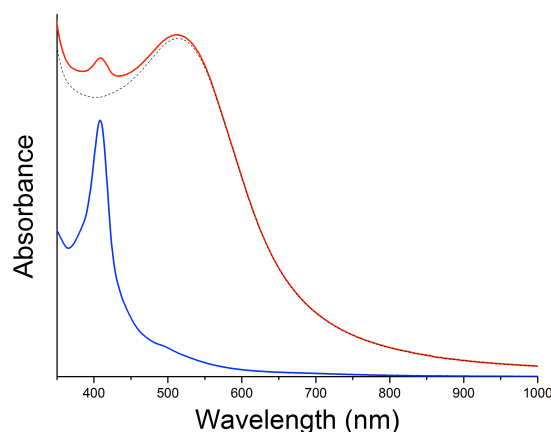


Figure S5. Optical absorption spectra of $M_3AuAg_{16}(TBBT)_{12}$ nanoparticles in DMF, with 1:16 (blue line) and 5:16 (red line) input ratios. The difference (dotted line) is also shown.

Theoretical Methodology

S5 - Density Functional Theory (DFT) and Time-Dependent DFT (TDDFT) Calculations:

The density functional theory (DFT) calculations for Bader charge analysis^{3,4} were performed using the VASP-DFT package with a plane-wave basis with a kinetic energy cutoff of 400 eV, PAW pseudopotentials,⁵ and the PW91 generalized gradient approximation (GGA) for the exchange-correlation potential.²⁻⁴ For structure optimization, convergence was achieved for forces smaller than 0.001 eV/Å. The rational design outlined in the text has been used as the starting point for the structural relaxation.

The calculations of the absorption spectra were carried out following the time-dependent density-functional theory (TDDFT) method with the formalism described in references^{5,6}, implemented in the real-space Octopus code.^{7,8} These calculations employed the norm-conserving non-local soft Troullier–Martins pseudopotentials⁹ (including the valence electrons for the elements in the molecule: Ag (4d¹⁰5s¹), S (3s² 3p⁴), C (2s² 2p²), H(1s¹), Na (3s¹)), using the generalized gradient-corrected PBE exchange–correlation (xc) potential.¹⁰

The Na₃Ag₁₇(TBBT)₁₂ structure (and those of the Au-substituted clusters) were relaxed with the use of the Born-Oppenheimer density functional theory (BODFT) code,¹¹ employing the above soft pseudopotentials and PBE xc potential. In the subsequent absorption spectra calculations the system was placed in a sphere of radius 21 Å such that the electron vanishes outside of that sphere. The grid spacing was taken as 0.2 Å, which corresponded to a 70 Ry plane-wave kinetic energy cutoff. The calculation involved 898 valence electrons. In the TDDFT calculations, we have used all states in the interval $E_F - 4.71$ eV to $E_F + 3.10$ eV, where the lower limit was chosen to coincide with a minimum in the density of states. This interval included 142 occupied states and 63 unoccupied states, and therefore 8946 electron-hole (occupied-unoccupied) pairs. Convergence was tested by varying the number of states included in the spectral calculations.

Detailed interpretation of the optical absorption spectrum requires analysis of the states and matrix elements contributing to the optical transition probabilities; see for example a method developed on the basis of time-dependent density functional perturbation theory (TD-DFPT) that allows analysis of correlations between single-particle transitions within a given energy range,¹⁶ which we have adopted in our analysis of the TDDFT results.

The measured and calculated absorption spectra for $\text{Na}_3\text{Ag}_{17}(\text{TBBT})_{12}$ in the optimal geometry (Fig. 2) are shown in **Fig. 3c** of the main text. In the calculated spectrum for the all-Ag cluster we find features at (A) 396 nm (3.13) originating from: (i) occupied states at -2.33 eV lying mostly on the phenyl rings, to the LUMO (0.89 eV) and LUMO+1 1D superatoms states on the metal core; (ii) occupied states on the S and Ag (d-states) atoms at -1.97 eV, to the 1D superatoms states, and (iii) the HOMO superatom 1P state to unoccupied states at 2.30 eV on the phenyl ring. For feature (B) the calculated peak occurs at 256 nm (4.85 eV), and it originates from: (i) phenyl π -states at -2.31 eV, to π^* -states at 2.51 eV hybridized in part with S states; (ii) d-band Ag and sulfur states at -1.97 eV, to phenyl and ligand states at 2.81 eV, and (iii) d-band metal states at -3.7 eV to -3.9 eV, to the unoccupied 1D superatom states near 1.01 eV.

For completeness we give here also the details of the calculations for $\text{Na}_3\text{Ag}_{17}(\text{SH})_{12}$
 Calculated peaks: A 422 nm (2.94 eV), B 262 nm (4.73 eV).

$E_{\text{gap}} = 2.04$ eV.

Energy range used in the TDDFT calculations $E_F - 5.70$ eV to $E_F + 3.74$ eV.

107 occupied states used in the calculations; 30 unoccupied states and 3210 electron-hole pairs.

Peak Origins:

A (HOMO-1) Superatom 1P states \rightarrow (LUMO +1) superatom 1D states.

B (-3.6 eV to -3.7 eV) d-band states \rightarrow LUMO+1 (1D superatom hybridized with S states).

In addition, we have carried out calculations for the mono-Au substituted cluster, $\text{Na}_3\text{AuAg}_{16}(\text{TBBT})_{12}$, as well as for cluster where the ligands have been replaced by SH groups, that is $\text{Na}_3\text{AuAg}_{16}(\text{SH})_{12}$. First, we display in Fig. S6 the measured and calculated spectra for $\text{Na}_3\text{AuAg}_{16}(\text{SR})_{12}$, SR = TBBT and SR = SH.

Details of the calculations in Fig. S6 are as follows:

$\text{Na}_3\text{AuAg}_{16}(\text{TBBT})_{12}$

Experimental peaks: A 408 nm (3.04 eV), B 281 nm (4.41 eV)

Calculated peaks: A 391 nm (3.17 eV), B 256 nm (4.85 eV)

Energy range used in the TDDFT calculations $E_F - 4.73$ eV to $E_F + 3.085$ eV

142 occupied states were used in the calculations; 63 unoccupied states and 8946 electron-hole pairs

The peak origins are the same as given in the text in the discussion of Fig. 3c

$\text{Na}_3\text{AuAg}_{16}(\text{SH})_{12}$

Calculated peaks: A 419 nm (2.96 eV), B 262 nm (4.73 eV)

$E_{\text{gap}} = 2.11$ eV

Energy range used in the TDDFT calculations $E_F - 5.76$ eV to $E_F + 3.650$ eV

107 occupied states used in the calculations; 30 unoccupied states and 3210 electron-hole pairs

Peak Origins:

A' (HOMO-1) Superatom 1P states \rightarrow (LUMO +1) superatom 1D states

B' (-3.6 eV to -3.7 eV) d-band states \rightarrow LUMO+1 (1Dsuperatom hybridized with S states).

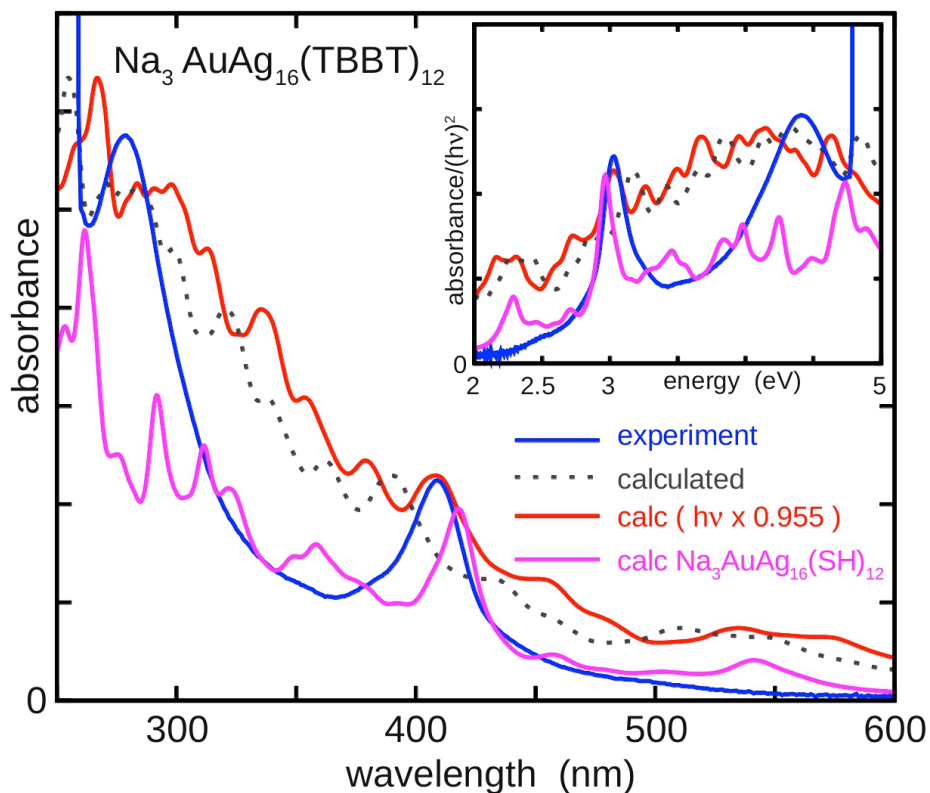


Figure S6. Measured (blue line) and TD-DFT calculated (red and dotted black lines) optical absorption spectra of $\text{Na}_3\text{AuAg}_{16}(\text{TBBT})_{12}$ nanoparticles, and calculated spectrum for $\text{Na}_3\text{AuAg}_{16}(\text{SH})_{12}$ (pink), plotted vs. wavelength and energy (inset). The dotted black line is the as-calculated spectrum, and the red line is obtained by scaling the as-calculated spectrum.

S6 - Structure of the Irregular (Distorted) Icosahedral-Shell (20 Triangles) Formed by the 12 Sulfur Atoms: The irregular icosahedral geometry of the 12 S atoms is shown in Fig. S4a. The 12 sulfur atoms (yellow) surround the silver core (13 Ag atoms, colored red), with three S atoms forming an equilateral triangle around each tetrahedrally-located Ag atom (4 Ag atoms colored green), to form a distorted icosahedron (yellow lines). There are 4 small equilateral triangles (12 E1 edges), 4 large equilateral triangles (12 E3 edges), and 6 pairs of large non-equilateral triangle having 6 common E2 edges. In the sulfur cage, each equilateral triangle made of the 3 sulfur atom that are bonded to an Ag atom shares its E1 edges with the non-equilateral triangles. The edge lengths of the 20 triangles that prescribe the distorted icosahedral cage made by the sulfur atoms are $E1 = 4.39 \text{ \AA} \pm 0.03 \text{ \AA}$, $E2 = 5.74 \text{ \AA} \pm 0.03 \text{ \AA}$, and $E3 = 6.54 \text{ \AA} \pm 0.06 \text{ \AA}$ (see Fig. S4b).

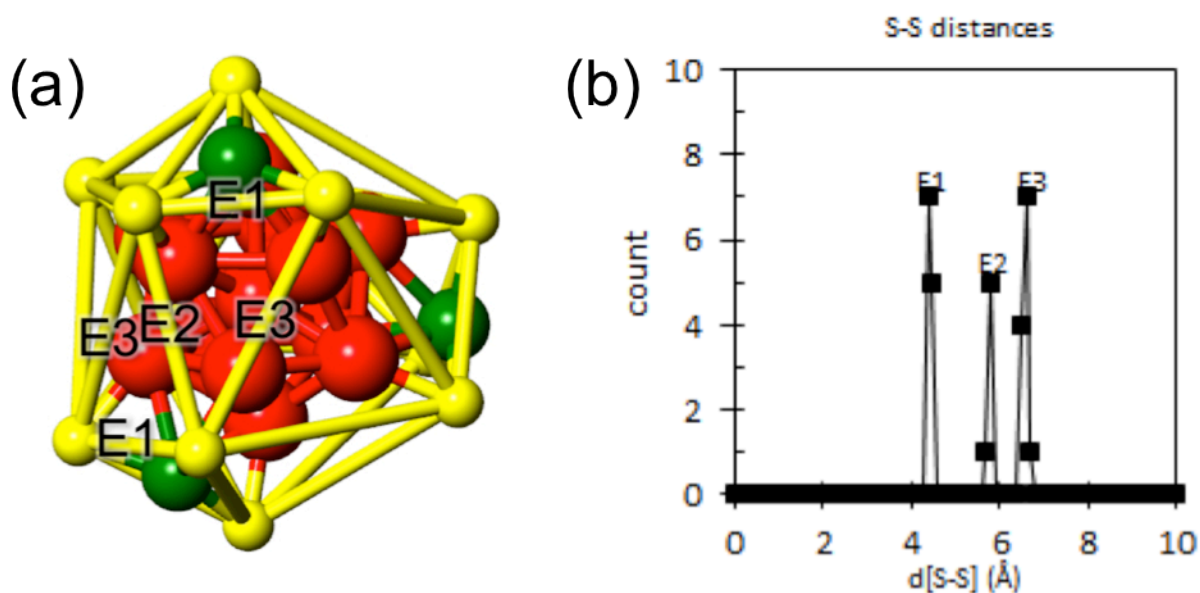


Figure S4. (a) Irregular icosahedral arrangement of 12 S atoms, composed of triangles with edge lengths E1, E2, and E3. Red spheres: 13 Ag atom icosahedral core; green spheres: tetrahedrally arranged 4 Ag atoms (part of the AgS_3 mounts); yellow spheres: 12 sulfur atoms. Connecting yellow sticks are drawn to visualize the irregular icosahedron formed by the 12 S atoms. (b) The S-S distances correspond to edge lengths E1, E2, and E3.

S7 - Bader Charge Analysis: The Bader charge analysis (BCA)^{3,4,17} provides an estimate of the local net charge in a prescribed region in the molecule by finding the difference between the number of electrons found in that region and the number of valence electrons associated with that region. Specifically, the BCA provides an estimate of the balance, $\Delta N(e^-)$, between the number of electrons, $N(e^-)$, found in a prescribed region about a selected atom or group of atoms and the number of valence electrons, $N_v(e^-)$, associated with that atom (or atoms) in that prescribed region when isolated from the molecule, such that $\Delta N(e^-) = N(e^-) - N_v(e^-)$ and the charge balance $\Delta Q(e^-) = -\Delta N(e^-)$.

The results of the BCA for $\text{Na}_3\text{Ag}_{17}(\text{TBBT})_{12}$ (Table S1) and $\text{Na}_4\text{Ag}_{44}(\text{p-MBA})_{30}$ (Table S2), show the excess electronic charge ($\Delta Q < 0$), deficiency ($\Delta Q > 0$), or no change ($\Delta Q = 0$) in the various prescribed regions of the molecule. The number of valence electrons considered in the pseudopotential for each of the elements was 11 for Ag, 6 for S, 4 for C, and 1 for H.

Table S1: Bader charge analysis for the optimal structure of $\text{Na}_3\text{Ag}_{17}(\text{TBBT})_{12}$

Region	$\Delta Q(e^-)$	$\Delta Q(e^-)/\text{unit}$
1 Ag (central)	-0.037	-0.037/atom
12 Ag (icosahedron)	1.606	0.134/atom
4 Ag (mounts)	1.240	0.310/atom
S	-4.326	-0.360/atom
C_6H_4	-2.172	-0.18/phenyl
C_4H_9	0.690	0.075/tertbutyl
3 Na	3	1/atom

Table S2: Bader charge analysis for the optimal structure of $\text{Na}_4\text{Ag}_{44}(\text{p-MBA})_{30}$ (see ref. 17)

Region	$N(e^-)$	$N_v(e^-)$	$\Delta Q(e^-)$	$\Delta Q(e^-)/\text{unit}$
12 Ag in inner shell	132.01	132	-0.01	-0.001/atom
8 Ag in outer shell (cube)	85.73	88	2.266	0.283/atom
12 Ag in outer shell	129.34	132	2.658	0.222/atom
12 Ag in mounts	127.91	132	4.09	0.341/atom
inner 24 S	152.53	144	-8.53	-0.355/atom
bridging 6 S	37.71	36	-1.71	-0.285/atom
30 Ph rings	838.38	840	1.618	0.054/Ph ring
30 COOH	334.39	330	-4.388	-0.146/COOH
4 Na	0	4	4	1/atom

The sum of all $\Delta Q = 0$, i.e. the 3 electrons on the $\text{Ag}_{17}(\text{TBBT})_{12}^{3-}$ ion came from the 3 Na atoms that became the Na^+ counterions. The total system (with the 3 Na^+) is charge neutral. Likewise, the 4 electrons on the $\text{Ag}_{44}(\text{p-MBA})_{30}^{4-}$ ion came from the 4 Na atoms that became the Na^+ counterions.

References:

- (1) Bakr, O. M.; Amendola, V.; Aikens, C. M.; Wenseleers, W.; Li, R.; Dal Negro, L.; Schatz, G. C.; Stellacci, F. *Angew. Chem. Int. Ed.* **2009**, *48*, 5921–5926.
- (2) Niedermeyer, T. H. J.; Strohm, M., *PLoS One* **2012**, *7* (9), 9.
- (3) Bader, R. F. W.: *Atoms in Molecules - A quantum theory*; Oxford University Press: New York, 1990.
- (4) Tang, W.; Sanville, E.; Henkelman, G. *J. Phys.: Condens. Matter* **2009**, *21*, 084204.
- (5) Kresse, G.; Joubert, D. *Phys. Rev. B* **1999**, *59*, 1758–1775.
- (6) Perdew, J. P. In *Electronic Structure of Solids '91*; Ziesche, P., Eschrig, H., Eds.; Akademie Verlag: Berlin, 1991; pp 11-20.
- (7) Perdew, J. P.; Chevary, J. A.; Vosko, S. H.; Jackson, K. A.; Pederson, M. R.; Singh, D. J.; Fiolhais, C. *Phys. Rev. B* **1992**, *46*, 6671-6687.
- (8) Perdew, J. P.; Chevary, J. A.; Vosko, S. H.; Jackson, K. A.; Pederson, M. R.; Singh, D. J.; Fiolhais, C. *Phys. Rev. B* **1993**, *48*, 4978-4978.
- (9) Casida, M. E. In *Recent Advances in Density Functional Methods, Part I*; Chong, D. P., Ed.; World Scientific: Singapore, 1995.
- (10) Casida, M. E. In *Recent Developments and Applications of Modern Density Functional Theory*; Seminario, J. M., Ed.; Elsevier: Amsterdam, 1996.
- (11) Marques, M. A. L.; Castro, A.; Bertsch, G. F.; Rubio, A. *Comput. Phys. Commun.* **2003**, *151*, 60–78.
- (12) Andrade, X.; Alberdi-Rodriguez, J.; Strubbe, D. A.; Oliveira, M. J. T.; Nogueira, F.; Castro, A.; Muguerza, J.; Arruabarrena, A.; Louie, S. G.; Aspuru-Guzik, A.; Rubio, A.; Marques, M. A. L. *J. Phys.: Condens. Matter* **2012**, *24*, 233202.
- (13) Troullier, N.; Martins, J. L. *Phys. Rev. B* **1991**, *43*, 1993-2006.
- (14) Perdew, J. P.; Burke, K.; Ernzerhof, M. *Phys. Rev. Lett.* **1996**, *77*, 3865-3868.
- (15) Barnett, R. N.; Landman, U. *Phys. Rev. B* **1993**, *48*, 2081-2097.
- (16) Yang, H.; Wang, Y.; Huang, H.; Gell, L.; Lehtovaara, L.; Malola, S.; Häkkinen, H.; Zheng, N. *Nat. Comm.* **2013**, *4*, 2422.
- (17) Desireddy, A.; Conn, B. E.; Guo, J.; Yoon, B.; Barnett, R. N.; Monahan, B. M.; Kirschbaum, K.; Griffith, W. P.; Whetten, R. L.; Landman, U.; Bigioni, T. P. *Nature* **2013**, *501*, 399-402.
- (18) Kumara, C.; Aikens, C. M.; Dass, A. *J. Phys. Chem. Lett.* **2014**, *5*, 461-466.